THE JOURNAL OF PHYSICAL CHEMISTRY C

Article

Cite This: J. Phys. Chem. C 2017, 121, 23398-23405

pubs.acs.org/JPCC

Orientation of Methylguanidinium Ions at the Water−Air Interface

S. Strazdaite,*[,†] J. Versluis,[†] N. Ottosson,[†,‡] and Huib J. Bakker*[,†]

[†]Institute for Atomic and Molecular Physics AMOLF, Science Park 102, Amsterdam 1098 XG, The Netherlands

[‡]Advanced Research Center for Nanolithography ARCNL, Science Park 110, Amsterdam 1098 XG, The Netherlands

Supporting Information

ABSTRACT: We use heterodyne-detected vibrational sum-frequency generation (HD-VSFG) to determine the orientation of the molecular plane of methylguanidinium ions at the surface of aqueous solutions. We measure the VSFG response of the symmetric and antisymmetric methyl stretch vibrations of the methylguanidinium ion with different polarization combinations. We find that for at least 50% of the methylguanidinium ions the molecular plane is at an angle >20° with respect to the surface plane. Hence, for only a minor fraction of the ions does the molecular plane have an orientation (near-)parallel to the surface plane, in contrast to the predictions of recent molecular dynamics simulation studies.

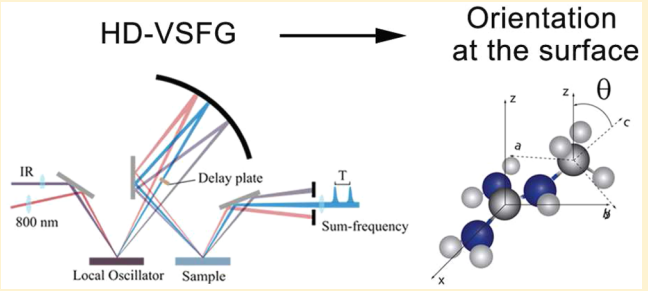

1. INTRODUCTION

The guanidinium cation ($C(NH_2)_3^+$ or Gdm^+) is one of the strongest and most widely used protein denaturants.[1] The mechanism underlying its exceptional protein unfolding capacity has been the subject of many experimental and theoretical studies.[2−4] The denaturation has been proposed to occur either (i) by indirect interactions mediated by ion-induced changes of the properties of the water solvent[2,5] or (ii) by direct interaction between the Gdm^+ ion and charged or aromatic protein side groups.[6,7]

The notion of an indirect mechanism strongly relies on the specific nature of the interaction between Gdm^+ and water, which has inspired a large number of studies on the structure of such solutions.[8−10] In particular, molecular dynamics simulations have given much insight into the ion's fascinating hydration properties.[7,11−13] Because of its planar shape and strongly nonuniform charge distribution, the Gdm^+ ion exhibits a highly anisotropic hydration structure. The net positive charge of the ion makes the lone pairs of the nitrogen atoms poor hydrogen-bond acceptors. As a result, there are few hydrogen bonds formed pointing perpendicular to the molecular plane, essentially rendering the ion hydrophobic along this molecular axis. The main hydration interactions of the Gdm^+ cation are directional hydrogen bonds donated by the N−H groups oriented in the plane of the ion. Consequently, the water solvent is more structured around Gdm^+ than around most other ions of similar size.

It has been suggested by several authors that the strong anisotropy of the hydration structure and the amphiphilic nature of the Gdm^+ ion are essential for how the ion binds to protein surfaces. While the ion can bind to negatively charged regions by strong in-plane hydrogen bonds, the out-of-plane hydrophobic interaction is thought to align Gdm^+ parallel to hydrophobic and aromatic patches. The strong ion−protein interaction resulting from this alignment has been considered to be an important factor in guanidinium's strong denaturation effect.[6,7,11] The out-of-plane hydrophobicity is even so severe that the existence of Gdm^+−Gdm^+ planar co-ion pairs has been proposed. In both classical and ab initio MD simulation studies, Gdm^+ ions have indeed been found to stack. This finding agrees with neutron scattering data.[7,12] This picture was later further experimentally supported by Shih et al.,[14] who showed that the red-shift of the nitrogen K-edge X-ray absorption spectroscopy (XAS) measurements could be theoretically reproduced from structures in which guanidinium ions form stacked co-ion pairs. Using quantum chemical calculations on the CCSD(T) level, Inagaki et al. found that such structures are stabilized through a subtle energy balance partly favorable because of π-stacking interactions and the reduction of hydrophobic effects, while partly unfavorable because of net repulsive Coulomb interactions.[15] Gdm^+−Gdm^+ co-ion pairing has further been invoked to explain the stabilizing role of arginine−arginine interactions on many protein surfaces.[16−18] While the somewhat unintuitive Gdm^+ co-ion pairing is becoming more and more accepted, this pairing is not supported by dielectric relaxation spectroscopy (DRS) and conductivity measurements.[10,19]

The anisotropic hydration properties of Gdm^+ lead to quite peculiar behavior of the ion near water−air interfaces. Overall, the water surface region shows a net depletion of guanidinium ions, resulting in an increased surface tension.[20] However, recent liquid-jet photoelectron spectroscopy experiments by Werner et al. showed that the concentration of guanidinium ions is enhanced at the surface itself, in the top molecular

Received: April 21, 2017
Revised: September 13, 2017
Published: September 14, 2017

DOI: 10.1021/acs.jpcc.7b03752
J. Phys. Chem. C 2017, 121, 23398−23405

layer.[21] MD simulation studies showed that surface-bound Gdm^+ ions show a strong preferential orientation parallel to the water surface, allowing for the formation of in-plane hydrogen bonds, while desolvating one of the hydrophobic faces.[22] Similar observations were made in MD simulations where slabs of GdmCl electrolytes were placed between either hydrophobic or hydrophilic plates.[23] The authors found that hydrophobic surfaces induce a stronger orientational parallel ordering of Gdm^+ ions than hydrophilic surfaces, thus further illustrating how the behavior of the ion at interfaces is driven by its anisotropic amphiphilic nature.

Recently, in a MD simulation study by Ou et al. the surface hydration properties of guanidinium were compared to those of methylguanidinium (M-Gdm^+, a derivative of Gdm^+).[24] In particular, the authors studied to what extent solute-induced interfacial solvent density fluctuations can explain the surface propensity of various orientational configurations of the solute, a topic which recently has attained significant attention for rationalizing the varying surface propensities of simple ions.[25−27] While the net surface activity of M-Gdm^+ and Gdm^+ was somewhat different, they found that both ions have primarily parallel-oriented configurations at the water surface.

In this work, we use heterodyne-detected vibrational sum frequency generation (HD-VSFG) to study the orientation of M-Gdm^+ ions at the water−air interface. HD-VSFG allows for the measurement of the absolute orientation of molecules at interfaces.[28,29] The point group symmetry of the Gdm^+ ion is D_{3h}, which implies that the ion possesses degenerate N−H vibrational modes of E' symmetry that should be VSFG active. However, the N−H stretch vibrations spectrally overlap with the relatively strong signal of the O−H stretch vibrations of water, thus making an analysis of these modes difficult. For M-Gdm^+, the methyl stretch vibrations can be clearly distinguished from the response of the water solvent, thus making this ion a much more suitable system to determine its orientation at the surface. By measuring the HD-VSFG response of the symmetric and antisymmetric stretch vibrations of the methyl group of M-Gdm^+ with different polarization combinations, we determine the orientation of the methyl group and thereby of the M-Gdm^+ ion at the water−air interface.

2. EXPERIMENT

The details of the HD-VSFG setup have been reported before.[30] Briefly, part of the pulses produced by a Ti:sapphire regeneratively amplified laser system (Coherent Legend, 1 kHz, ∼35 fs, ∼3.5 mJ, 800 nm at 1 kHz) is used to produce broadband infrared (IR) pulses (tunable from 2 to 10 μm) with a home-built optical parametric amplifier. The remaining part of the 800 nm fundamental is spectrally narrowed using an etalon (bandwidth ∼15−20 cm^{-1}) and is spatially and temporally overlapped with the broadband IR pulse to generate sum-frequency light from the surface of a local oscillator, in this case a gold mirror (Thorlabs model PF 10-03-M01). The generated LO-SFG light is then delayed in time using a silica plate and is focused onto the surface of the sample under study, together with the remaining IR and visible (VIS) 800 nm beams. At the sample surface the IR and VIS pulses again generate sum-frequency light. This VSFG light and the LO-SFG beam are recollimated and sent into a monochromator where they interfere, the degree of which depends on their phase relation. The interference pattern is detected with a CCD camera (EMCCD, Andor Technologies). The incident angles of the IR, VIS, and SFG beams (with respect to the surface normal) at the sample are 40°, 35°, and 36°, respectively.

The expression for the final detected VSFG interference pattern contains cross terms between LO-SFG light and VSFG light generated from the sample, which we extract by Fourier filtering.[30] To remove the SFG contribution from the local oscillator and correct for the frequency-dependent intensity variations of the IR pulse, we normalize the spectra from the sample by dividing them by a reference spectrum, obtained from a z-cut α-quartz crystal. To determine the absolute sign of HD-VSFG and to evaluate relative intensities, the effective susceptibility of quartz in different polarization combinations needs to be accurately known. In a copropagating reflective geometry, the effective susceptibilities of quartz in SSP and in PPP polarization configurations have the same sign, even though the macroscopic second-order susceptibilities have different signs.[31] Because of differences in Fresnel factors, the effective susceptibility in SSP and PPP do not have the same values. In our experimental geometry $\chi_{eff}^{(2),SSP}/\chi_{eff}^{(2),PPP} \cong 1.14$ for quartz in the 3000 cm^{-1} region. It is also crucial that the HD-VSFG signal obtained from z-cut quartz is generated at the same height as the HD-VSFG signal from the sample, as height differences would introduce phase errors. The height can be controlled by monitoring the location of the signal on the CCD camera, leading to an estimated phase uncertainty of $\sim\pi/10$ (∼20°).

The samples (3 M methylguanidine hydrochloride) were prepared from mixing D_2O (≥99.96%, Cambridge Isotope Laboratories) and methylguanidine hydrochloride (≥98%, Sigma-Aldrich).

3. THEORY: VSFG SIGNAL OF A METHYL GROUP

3.1. Relation between the VSFG Signal and the Molecular Hyperpolarizability. To determine the orientation of molecular groups at interfaces with VSFG, we need to relate the effective nonlinear susceptibility $\chi_{eff}^{(2)}$ to the microscopic molecular hyperpolarizability $\beta_{i'j'k'}$ tensor elements. This relation can be found in the literature.[32−37] Here we present this relation for the C_{3v} symmetry molecular group at rotationally isotropic achiral interfaces ($C_{\infty v}$).

In VSFG spectroscopy the generated electric field at the sum-frequency is proportional to the electric fields of the incident IR and VIS beams and the effective second-order nonlinear susceptibility $\chi_{eff}^{(2)}$:

$$E_{SFG}(\omega) = \chi_{eff}^{(2)}(\omega) E_{VIS}(\omega_1) E_{IR}(\omega_2) \quad (1)$$

here ω, ω_1, and ω_2 are the frequencies of sum-frequency, visible, and infrared light, respectively. $E_{SFG}(\omega)$, $E(\omega_1)$, and $E(\omega_2)$ are the strengths of those respective electric fields. We define the laboratory coordinates with the z-axis as the surface normal and with x and y forming the rotationally symmetric surface plane. All beams propagate in the x,z plane; thus, p-polarization denotes the polarization of the optical field in x,z plane, while s-polarization is along the y-axis, perpendicular to the x,z plane.

In total, the $\chi_{ijk}^{(2)}$ tensor can have 27 elements, but because of symmetry considerations interfaces with $C_{\infty v}$ symmetry (achiral rotationally isotropic) have only 7 nonzero tensor elements, of which only 4 are independent: $\chi_{xxz}^{(2)} = \chi_{yyz}^{(2)}$, $\chi_{xzx}^{(2)} = \chi_{yzy}^{(2)}$, $\chi_{zxx}^{(2)} = \chi_{zyy}^{(2)}$, and $\chi_{zzz}^{(2)}$. These four components can be deduced by measuring SFG intensities with different input and output polarization combinations, such as SSP, SPS, PSS, and PPP, where the

DOI: 10.1021/acs.jpcc.7b03752
J. Phys. Chem. C 2017, 121, 23398−23405

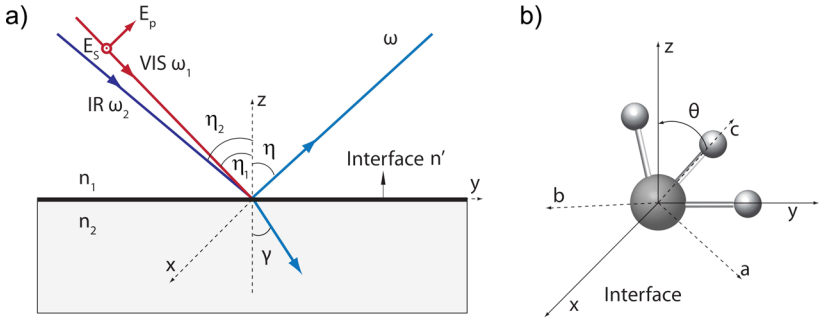

Figure 1. (a) Geometry of our VSFG experiment in a Cartesian lab coordinate system. The incident and emitted beams propagate in the *x*,*z* plane. (b) Molecular coordinates (*a*, *b*, *c*) and laboratory coordinates (*x*, *y*, *z*), relevant for the methyl group at water surfaces. The angle θ denotes the tilt angle between the methyl C_3 main symmetry axis (*c*-axis) and the surface normal *z*.

respective positions refer to the polarization of the contributing SFG, VIS, and IR beams, respectively. SSP polarization probes only one tensor element $\chi^{(2)}_{xxz}$, whereas PPP probes combination of all four independent tensor elements. $\chi^{(2)}_{\text{eff}}$ for those four polarization combinations are related to all the nonzero seven $\chi^{(2)}_{ijk}$ tensor elements:[34,37]

$$\begin{aligned}
\chi^{(2),\text{SSP}}_{\text{eff}} &= L_{yy}(\omega)L_{yy}(\omega_1)L_{zz}(\omega_2)\sin\eta_2\chi^{(2)}_{xxz}\\
\chi^{(2),\text{SPS}}_{\text{eff}} &= L_{yy}(\omega)L_{zz}(\omega_1)L_{yy}(\omega_2)\sin\eta_1\chi^{(2)}_{xzx}\\
\chi^{(2),\text{PSS}}_{\text{eff}} &= L_{zz}(\omega)L_{yy}(\omega_1)L_{yy}(\omega_2)\sin\eta\chi^{(2)}_{zxx}\\
\chi^{(2),\text{PPP}}_{\text{eff}} &= -L_{xx}(\omega)L_{xx}(\omega_1)L_{zz}(\omega_2)\cos\eta\cos\eta_1\sin\eta_2\chi^{(2)}_{xxz}\\
&\quad -L_{xx}(\omega)L_{zz}(\omega_1)L_{xx}(\omega_2)\cos\eta\sin\eta_1\cos\eta_2\chi^{(2)}_{xzx}\\
&\quad +L_{zz}(\omega)L_{xx}(\omega_1)L_{xx}(\omega_2)\sin\eta\cos\eta_1\cos\eta_2\chi^{(2)}_{zxx}\\
&\quad +L_{zz}(\omega)L_{zz}(\omega_1)L_{zz}(\omega_2)\sin\eta\sin\eta_1\sin\eta_2\chi^{(2)}_{zzz}
\end{aligned} \tag{2}$$

Here, η_i is the incident angle of the optical field E_i. $L_{ii}(i = x, y, z)$ are Fresnel coefficients determined by the refractive indices of the two media ($n_1(\omega_i)$ and $n_2(\omega_i)$) and the interface layer ($n'(\omega_i)$), and the incident (η_i) and reflected angles (γ_i):

$$\begin{aligned}
L_{xx}(\omega_i) &= \frac{2n_1(\omega_i)\cos\gamma_i}{n_1(\omega_i)\cos\gamma_i + n_2(\omega_i)\cos\eta_i}\\
L_{yy}(\omega_i) &= \frac{2n_1(\omega_i)\cos\beta_i}{n_1(\omega_i)\cos\eta_i + n_2(\omega_i)\cos\gamma_i}\\
L_{zz}(\omega_i) &= \frac{2n_2(\omega_i)\cos\eta_i}{n_1(\omega_i)\cos\gamma_i + n_2(\omega_i)\cos\eta_i}\left(\frac{n_1(\omega_i)}{n'(\omega_i)}\right)^2
\end{aligned} \tag{3}$$

The second-order susceptibilities are determined by the microscopic hyperpolarizabilities $\beta_{i'j'k'}$ ($i'j'k' = a, b, c$; molecular coordinates, see Figure 1b). From a quantum mechanical treatment, using perturbation theory of the electron wave function, it can be shown that hyperpolarizability tensor elements of a particular vibrational mode *q* are proportional to the Raman polarizability ($\alpha_{i'j'}$) derivative and dipole moment ($\mu_{k'}$) derivative tensor elements:[32,38]

$$\beta^{(2)}_{i'j'k'} = -\frac{1}{2\epsilon_0\omega_q}\frac{\mathrm{d}\alpha_{i'j'}}{\mathrm{d}Q_q}\frac{\mathrm{d}\mu_{k'}}{\mathrm{d}Q_q} \tag{4}$$

where ω_q and Q_q are the resonant vibrational frequency and the normal coordinates of *q*th vibrational mode and ϵ_0 denotes vacuum permittivity. The macroscopic susceptibility $\chi^{(2)}_{ijk}$ is an ensemble average of the microscopic hyperpolarizabilities and can be written as

$$\chi^{(2)}_{ijk} = \frac{N_S}{\epsilon_0}\sum_{i'j'k'}\langle R_{ii'}R_{jj'}R_{kk'}\rangle\beta^{(2)}_{i'j'k'} \tag{5}$$

where N_s is the number density of the molecules probed at the interface. $R_{\lambda\lambda'}$ is the element of the rotational transformation matrix used to convert from the molecular coordinates (*a*, *b*, *c*) to surface bound coordinates (*x*, *y*, *z*). The $\chi^{(2)}_{ijk}$ and $\beta_{i'j'k'}$ can be connected using the symmetry of the molecular vibration and performing an Euler transformation for all three angles (θ, ϕ, ψ). For the methyl group with C_{3v} symmetry, we naturally choose the *c*-axis along the symmetry axis of the C_3 methyl group, and the *a* and *b* axes form a plane perpendicular to the *c*-axis. The *a*-axis is along one of the C−H bonds (see Figure 1b). There are 11 nonzero molecular hyperpolarizability elements for the methyl group (of which 4 are independent); 3 for the symmetric vibration ($\beta_{aac} = \beta_{bbc}$, β_{ccc}) and 8 for the antisymmetric vibration ($\beta_{aca} = \beta_{bcb}$, $\beta_{caa} = \beta_{cbb}$, $\beta_{aaa} = -\beta_{bba} = -\beta_{abb} = -\beta_{bab}$).[39] We have for the symmetric vibration

$$\begin{aligned}
\chi^{(2),\text{ss}}_{xxz} &= \frac{1}{2}N_s\beta_{ccc}\langle\cos\theta\rangle[(1+R)-(1-R)D]\\
\chi^{(2),\text{ss}}_{xzx} &= \chi^{(2),\text{ss}}_{zxx} = \frac{1}{2}N_s\beta_{ccc}(1-R)\langle\cos\theta\rangle[1-D]\\
\chi^{(2),\text{ss}}_{zzz} &= N_s\beta_{ccc}\langle\cos\theta\rangle[R+(1-R)D\rangle]
\end{aligned} \tag{6}$$

and for the antisymmetric vibration

$$\begin{aligned}
\chi^{(2),\text{as}}_{xxz} &= -N_s\beta_{aca}\langle\cos\theta\rangle(1-D)\\
\chi^{(2),\text{as}}_{xzx} &= \chi^{(2),\text{as}}_{zxx} = N_s\beta_{aca}\langle\cos\theta\rangle D\\
\chi^{(2),\text{as}}_{zzz} &= 2N_s\beta_{aca}\langle\cos\theta\rangle(1-D)
\end{aligned} \tag{7}$$

where θ is the tilt angle between the methyl C_3 axis and the surface normal *z* and *R* is the ratio of the hyperpolarizability elements, $R = \beta_{\text{aac}}/\beta_{\text{ccc}}$. *D* is an orientational parameter, defined as

$$D = \frac{\langle\cos^3\theta\rangle}{\langle\cos\theta\rangle} \tag{8}$$

DOI: 10.1021/acs.jpcc.7b03752
J. Phys. Chem. C 2017, 121, 23398−23405

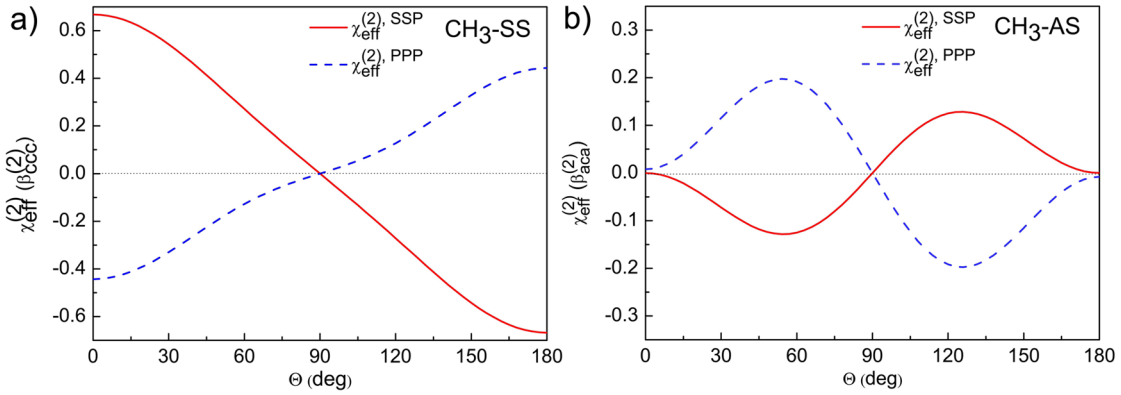

Figure 2. Calculated $\chi^{(2)}_{eff}$ (β_{ccc}) as a function of the orientational angle θ for the symmetric methyl vibration assuming that $R = 2$ (a) and $\chi^{(2)}_{eff}$ (β_{aca}) for the antisymmetric methyl vibration (b). The results are plotted for SSP and PPP polarization combinations. The details of the calculations are given in the text.

If one assumes that the orientation distribution function is a δ-function, the tilt angle (θ_δ) is

$$\theta_\delta = \arccos(\sqrt{D}) \tag{9}$$

It follows from from eqs 6 and 7 that the ratios of the signals measured for different vibrations, for example the symmetric and the antisymmetric vibration, depend on only θ, via D. Hence, D is the crucial parameter to be obtained from the VSFG measurements to determine the molecular orientation of the methyl group at the water surface.

3.2. Dependence of the VSFG Signal on the Orientation Angle. The formalism presented in the section 3.1 provides the relation between the effective second-order susceptibilities $\chi^{(2)}_{eff}$ measured with HD-VSFG with different polarization combinations and the orientation of the CH_3 group relative to the water surface. To make such a comparison several optical parameters of the system need to be determined.

The Fresnel coefficients depend on the refractive indices of the sum-frequency, the 800 nm and the mid-infrared light at ~2900 cm^{-1}. The refractive indices of the 800 nm and the sum-frequency (~645 nm) beams show very little change with frequency and solute concentration, as neither D_2O nor methylguanidinium possesses resonances in the visible. For both the 800 nm beam and the sum-frequency beam we use a refractive index of 1.47, as reported by Sigma Aldrich for solutions of guanidinium in D_2O (8 M concentration). The refractive index at the mid-infrared frequency of ~2900 cm^{-1} will be strongly frequency and concentration dependent, as this frequency is resonant with the C−H vibrations of methylguanidinium and close to vibrational resonances of D_2O. We determined the refractive index around 2900 cm^{-1} of a solution of 3 M methylguanidinium in D_2O from the spacing of the Fabry−Perot fringes in the infrared spectrum and arrived at a value of 2.17.

An important parameter in the Fresnel coefficient L_{zz} is the refractive index n' of the interfacial layer (Figure 1a).[34] In some studies, n' was taken to be equal to that of the bulk medium value (n_2),[40,41] while in others it was determined using experimental techniques such as ellipsometry.[42] Shen et al. derived a formalism for estimating n' when n_2 is known, using a modified Lorentz model for local field correction at the interface, and showed that such a model can be used to determine the molecular orientation of pentyl-cyanoterphenyl molecules at the air−water interface.[34] Using this method we obtain a value for n' of 1.16 at 800 nm and sum-frequency and 1.48 at the mid-infrared frequency around 2900 cm^{-1}. We neglect the dispersion of the refractive indexes and use the same values for all frequencies within the VSFG spectrum.

Hyperpolarizability $\beta_{i'j'k'}$ tensor elements (β_{aac}, β_{aca}, β_{ccc}) can be calculated by the so-called bond additivity method, also called the bond polarizability derivative model, which was first derived by Hirose et al.[32,39] From this formalism follows that $4 > R > 1$. The exact value of R depends on the molecule to which the methyl group belongs. More recently, ab initio calculations have been employed to determine hyperpolarizability tensor elements.[43] We determine R from the fit of the experimental data.

Figure 2 shows calculated $\chi^{(2)}_{eff}$ values for the symmetric (SS) and antisymmetric (AS) methyl stretch vibrations in both SSP and PPP polarization combinations, plotted as a function of the angle θ (see Figure S1 in Supporting Information for SPS polarization combination) assuming a δ-distribution function for θ. It is important to note that for the SS mode the calculated intensity has β_{ccc} as a unit, and the AS mode has β_{aca} as a unit. Hence, the scales of graphs in Figure 2a,b cannot be compared directly, unless the absolute values of hyperpolarizability tensor elements are known. The ratio β_{aca}/β_{ccc} can acquire quite different values depending on the system studied. For instance, β_{aca}/β_{ccc} was found to be 0.4 for methanol and 4.5 for ethanol.[44] Hence, we will use this ratio as a fit parameter S ($=\beta_{aca}/\beta_{ccc}$) in describing the experimental spectra.

It follows from Figure 2 that for the symmetric mode, the imaginary $\chi^{(2)}$ measured with SSP is always at least ~1.5 times higher than the imaginary $\chi^{(2)}$ measured with PPP and that the sign is opposite for the two polarization combinations. For the antisymmetric mode the intensity is larger in PPP than in SSP (~2 times) and the sign is also opposite in the two polarization combinations.

4. RESULTS AND DISCUSSION

In Figure 3 we show imaginary $\chi^{(2)}$ spectra of 3 M methylguanidinium hydrochloride solutions measured with SSP and PPP polarization combinations. As M-Gdm^+ possesses a single methyl group, there will be three modes contributing to the signal in this frequency region: the symmetric stretch vibration (SS), the Fermi resonance (FR), and the antisymmetric stretch vibration (AS). The Fermi resonance results from the interaction between the symmetric methyl vibration and the overtone of the bending mode (~1460 cm^{-1}). Following previous work, we label the band at 2922 cm^{-1} as

DOI: 10.1021/acs.jpcc.7b03752
J. Phys. Chem. C 2017, 121, 23398−23405

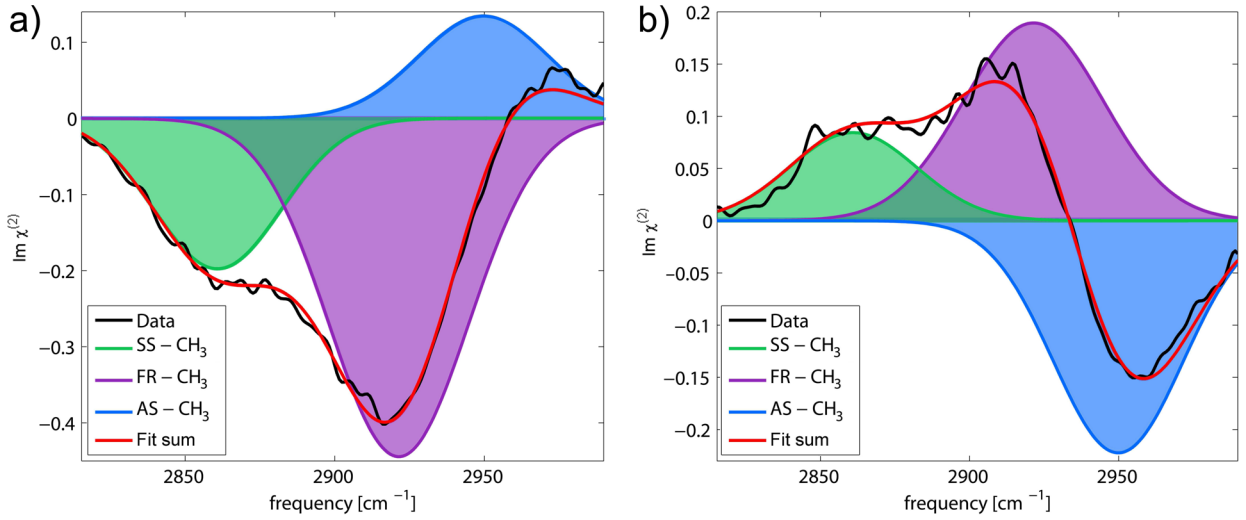

Figure 3. Imaginary $\chi^{(2)}$ spectra of methylguanidine hydrochloride at different polarization combinations: SSP (a) and PPP (b). The global fitting result is shown as the red line, and the contributions of the separate Gaussian peaks are represented by the different colors.

the Fermi resonance (FR) band. However, both bands (SS and FR) contain symmetric stretch vibrational character, and this character determines the VSFG cross section of these bands. The band at 2863 cm^{-1} is the lower-frequency band of the Fermi split symmetric stretch, and the band at 2922 cm^{-1} is the higher-frequency band of the Fermi split symmetric stretch. It follows that both bands have the same symmetry and that the total amplitude of the symmetric methyl stretch vibration is represented by the sum of the amplitudes of the two bands. The sign of the SS and the FR bands thus shows the same dependence on the polarization combination. The peak at ~2946 cm^{-1} shows opposite behavior, and we assign this band to the AS mode.

Using the dependence of the VSFG signal of the different vibrations on the orientational angle (illustrated in Figure 2), we can now fit the experimental data (Figure 3). In this fit we determine the center frequencies and widths of the AS, FR, and SS peaks, the R and S parameters describing the hyperpolarizability ratios ($R = \beta_{aac}/\beta_{ccc}$, $S = \beta_{aac}/\beta_{aca}$), the parameter D that describes the orientation of the methyl group, a parameter that defines the ratio of the FR and SS peaks and an overall scaling parameter. The relative peak intensities of the SS bands in the two polarization combinations are described by the R and D parameters. The FR bands have the same ratio as the SS bands in the two polarization combinations. The relative peak intensities of the AS bands in the two polarization combination is defined only by the D parameter. Within each polarization combination, the ratio of SS and FR with respect to AS is determined by the S parameter.

The resulting fit parameters are given in Table 1, and the result of the fit is plotted together with the experimental data in Figure 3. For R we obtain a value of 1.0 ± 0.1, and for S a value of 1.1 ± 0.1, which implies that the three hyperpolarizability tensor elements β_{aac}, β_{aca}, and β_{ccc} would be quite similar in size for the M-Gdm$^+$ ion. For D we find a value of 0.5 ± 0.06.

The orientation dependence of the VSFG signals of the three different modes in the SSP and PPP experiments is expressed in the value of D. It should be realized that the same value of D can result from different angular distributions. To explore the range of possible angular distributions, we define the distribution as a Gaussian function with central angle θ_c, which has zero amplitude for $\theta > 90°$. This distribution can be rationalized by considering the hydrophobic nature of the methyl group, making it unlikely that surface-bound M-Gdm$^+$ would orient such that the methyl group would be pointing toward the bulk aqueous phase, i.e. $\theta > 90°$. We will refer to such a distribution as a partial-Gaussian, defined as

$$F_{PG}(\theta) = \begin{cases} \exp[-4\ln 2(\theta - \theta_c)^2/\sigma^2] & \text{if } 0° < \theta < 90° \\ 0 & \text{if } 90° < \theta < 180° \end{cases} \quad (10)$$

D can be evaluated for this distribution using

$$D = \frac{\int_{0°}^{90°} \cos^3\theta \sin\theta F_{PG}(\theta)\, d\theta}{\int_{0°}^{90°} \cos\theta \sin\theta F_{PG}(\theta)\, d\theta} \quad (11)$$

In Figure 4a the orientational parameter D (calculated from eq 11) is plotted as a function of the center angle θ_c for three different widths σ (20°, 50°, and 90°) of partial-Gaussian distribution function. In Figure 4b, D is shown as a function of the width σ for θ_c equal to 45° and 90°. In case the angular distribution would be a δ-function (zero width), the D value of 0.5 ± 0.06 would correspond to a molecular tilt angle θ_c of 45° ± 2°. For $\theta_c = 90°$, a minimum width of 150° is required to obtain the experimentally determined D value of 0.5 ± 0.06. Figure 4c illustrates the distribution with $\theta_c = 90°$, a width of 150°, and a δ-distribution at $\theta = 45°$. In the Supporting Information we compare calculations for a partial-Gaussian distribution with a full-Gaussian distribution (no truncation at $\theta = 90°$ in eq 10; see Figure S3).

Table 1. Parameters Determined from a Global Fit of the SSP and PPP Spectra of M-Gdm$^+$

	R	1.0 ± 0.1
	S	1.1 ± 0.1
	D	0.5 ± 0.06
SS	ω_{SS}	2863 cm^{-1}
	σ_{SS}	23 cm^{-1}
FR	ω_{FR}	2922 cm^{-1}
	σ_{FR}	23 cm^{-1}
AS	ω_{AS}	2950 cm^{-1}
	σ_{AS}	21 cm^{-1}

DOI: 10.1021/acs.jpcc.7b03752
J. Phys. Chem. C 2017, 121, 23398−23405

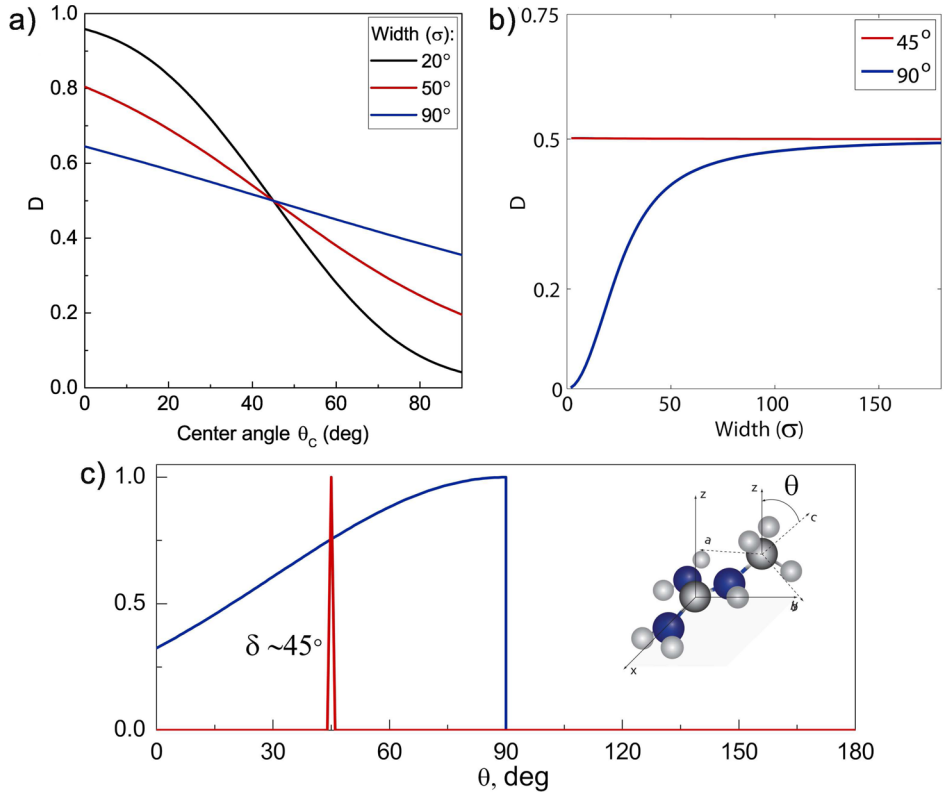

Figure 4. Dependence of D on the center angle of the partial-Gaussian distribution as defined in eq 11 for three different widths σ (a). D as a function of the width (σ) for 45° and 90° center angles (b). A partial-Gaussian angular distributions with θ_c = 90° and a width of ~150° and δ-function at 45° (c).

The orientation of Gdm^+ and M-Gdm^+ cations at the water−air interface has been investigated by Ou et al. using MD simulations.[24,27] These MD simulations find the most probable surface-bound configuration to be parallel to the surface flat, which can be described with a partial-Gaussian with center angle θ_c = 90°. Interestingly, further toward the vapor phase, the simulations of M-Gdm^+ show that the ion has a tendency to orient with its methyl group pointing away from the liquid phase, corresponding to configurations with tilt angles θ close to 0°. The density profiles reported by Ou et al. further suggest that the relative contribution from M-Gdm^+ in the vapor phase is rather small,[27] which corresponds to a partial-Gaussian with center angle θ_c = 90° and a relatively narrow width.

The experimentally observed D can be reproduced with a partial-Gaussian distribution with center angle θ_c = 90° in case this distribution has a large width of ~150°. This width implies that ~80% of the M-Gdm^+ ions are oriented at an angle >20° with respect to the surface plane. For all possible center angle θ_c and width σ combitions yielding D = 0.5, the fraction of molecules that are at an angle >20° with respect to the surface plane is at least ~50%. This notion applies both to the partial-Gaussian and a full-Gaussian distributions (see the Supporting Information). Hence, the VSFG results show that M-Gdm^+ ions at the water−air interface are oriented less parallel to the water−air interface than has been predicted by MD simulations.[27]

5. CONCLUSIONS

We presented a heterodyne-detected vibrational surface sum-frequency generation study of the orientation of methylguanidinium ions at the water−air interface. To this purpose, we measured HD-VSFG spectra of the symmetric and antisymmetric methyl stretch vibrations of the ion in SSP and PPP polarization combinations. From these spectra we obtained the ratios of the second-order susceptibility tensor elements that provide information on the molecular orientation of the probed methyl group. Assuming a δ-distribution for the orientation angle, we find that the observed spectra can be well explained if the C_3 axis of the methyl group of methylguanidinium is at an angle of ~45° with respect to the surface normal. Assuming a partial-Gaussian orientational distribution with its maximum at 90° (= parallel to the surface plane), we find that the spectra can be explained only if this distribution has a width of at least ~150°. From this, we conclude that for ~80% of the methylguanidinium ions the molecular plane is at an angle >20° with respect to the surface plane, which implies that only a minor fraction of the ions have an orientation (near-)parallel to the water surface. We find that at least 50% of methylguanidinium ions are oriented at an angle >20° with respect to the surface plane.

■ ASSOCIATED CONTENT

Supporting Information

The Supporting Information is available free of charge on the ACS Publications website at DOI: 10.1021/acs.jpcc.7b03752.

Details of fitting SSP and PPP spectra of methylguanidinium; calculated $\chi^{(2)}_{eff}$ versus orientational angle θ for symmetric and antisymmetric methyl vibration in SSP, SPS, and PPP polarization combinations (Figure S1); deviations of the fitted SSP and PPP spectra if R or D changes within the range of errors, determined from fitting (Figure S2); comparison of partial and full-

DOI: 10.1021/acs.jpcc.7b03752
J. Phys. Chem. C 2017, 121, 23398−23405

Gaussian distributions for dependence of D on the angle θ_c of the maximum of the distribution for three different widths, width of the distribution required to get a D value of 0.5 as a function of θ_c, and the fraction of molecules with their main axis at an angle $\theta > 20°$ with respect to the surface plane for different values of θ_c (Figure S3)(PDF)

AUTHOR INFORMATION

Corresponding Authors

*E-mail: strazdaite@amolf.nl.
*E-mail: bakker@amolf.nl.

ORCID

S. Strazdaite: 0000-0003-0007-5507

Notes

The authors declare no competing financial interest.

ACKNOWLEDGMENTS

This work is part of the research program of the "Stichting voor Fundamenteel Onderzoek der Materie (FOM)", which is financially supported by the "Nederlandse organisatie voor Wetenschappelijk Onderzoek (NWO)". The work was performed within the framework of a FOM Industrial Partnership Program with Top-institute Wetsus for water research and is also financially supported by Wetsus.

REFERENCES

(1) Arakawa, T.; Timasheff, S. N. Protein Stabilization and Destabilization by Guanidinium Salts. *Biochemistry* **1984**, *23*, 5924−5929.

(2) Schiffer, C. A.; Dötsch, V. The Role of Protein-Solvent Interactions in Protein Unfolding. *Curr. Opin. Biotechnol.* **1996**, *7*, 428−432.

(3) Alonso, D. O. V.; Dill, K. A. Solvent Denaturation and Stabilization of Globular Proteins. *Biochemistry* **1991**, *30*, 5974−5985.

(4) Shukla, D.; Schneider, C. P.; Trout, B. L. Complex Interactions between Molecular Ions in Solution and Their Effect on Protein Stability. *J. Am. Chem. Soc.* **2011**, *133*, 18713−18718.

(5) Scott, J. N.; Nucci, N. V.; Vanderkooi, J. M. Changes in Water Structure Induced by the Guanidinium Cation and Implications for Protein Denaturation. *J. Phys. Chem. A* **2008**, *112*, 10939−10948.

(6) O'Brien, E. P.; Dima, R. I.; Brooks, B.; Thirumalai, D. Interactions between Hydrophobic and Ionic Solutes in Aqueous Guanidinium Chloride and Urea Solutions: Lessons for Protein Denaturation Mechanism. *J. Am. Chem. Soc.* **2007**, *129*, 7346−7353.

(7) Mason, P. E.; Dempsey, C. E.; Neilson, G. W.; Kline, S. R.; Brady, J. W. Preferential Interactions of Guanidinum Ions with Aromatic Groups over Aliphatic Groups. *J. Am. Chem. Soc.* **2009**, *131*, 16689−16696.

(8) Miyajima, K.; Yoshida, H.; Kuroda, Y.; Nakagaki, M. Studies on the Aqueous Solutions of Guanidinium Salts. XIII. NMR Study of the Interactions between Guanidinium Salt and Tetraalkylammonium Salts in Water. *Bull. Chem. Soc. Jpn.* **1980**, *53*, 2212.

(9) Vorobyev, D. Y.; Kuo, C.-H.; Chen, J.-X.; Kuroda, D. G.; Scott, J. N.; Vanderkooi, J. M.; Hochstrasser, R. M. Ultrafast Vibrational Spectroscopy of a Degenerate Mode of Guanidinium Chloride. *J. Phys. Chem. B* **2009**, *113*, 15382−15391.

(10) Hunger, J.; Niedermayer, S.; Buchner, R.; Hefter, G. Are Nanoscale Ion Aggregates Present in Aqueous Solutions of Guanidinium Salts? *J. Phys. Chem. B* **2010**, *114*, 13617−13627.

(11) Mason, P. E.; Neilson, G. W.; Enderby, J. E.; Saboungi, M.-L.; Dempsey, C. E.; MacKerell, A. D.; Brady, J. W. The Structure of Aqueous Guanidinium Chloride Solutions. *J. Am. Chem. Soc.* **2004**, *126*, 11462−11470.

(12) Vazdar, M.; Uhlig, F.; Jungwirth, P. Like-Charge Ion Pairing in Water: An Ab Initio Molecular Dynamics Study of Aqueous Guanidinium Cations. *J. Phys. Chem. Lett.* **2012**, *3*, 2021−2024.

(13) England, J. L.; Haran, G. Role of Solvation Effects in Protein Denaturation: From Thermodynamics to Single Molecules and Back. *Annu. Rev. Phys. Chem.* **2011**, *62*, 257−277.

(14) Shih, O.; England, A. H.; Dallinger, G. C.; Smith, J. W.; Duffey, K. C.; Cohen, R. C.; Prendergast, D.; Saykally, R. J. Cation-Cation Contact Pairing in Water: Guanidinium. *J. Chem. Phys.* **2013**, *139*, 035104−7.

(15) Inagaki, T.; Aono, S.; Nakano, H.; Yamamoto, T. Like-Charge Attraction of Molecular Cations in Water: Subtle Balance between Interionic Interactions and Ionic Solvation Effect. *J. Phys. Chem. B* **2014**, *118*, 5499−5508.

(16) Pednekar, D.; Tendulkar, A.; Durani, S. Electrostatics-Defying Interaction between Arginine Termini as a Thermodynamic Driving Force in Protein-Protein Interaction. *Proteins: Struct., Funct., Genet.* **2009**, *74*, 155−163.

(17) Neves, M. A. C.; Yeager, M.; Abagyan, R. Unusual Arginine Formations in Protein Function and Assembly: Rings, Strings, and Stacks. *J. Phys. Chem. B* **2012**, *116*, 7006−7013.

(18) Vazdar, M.; Vymětal, J.; Heyda, J.; Vondrášek, J.; Jungwirth, P. Like-Charge Guanidinium Pairing from Molecular Dynamics and Ab Initio Calculations. *J. Phys. Chem. A* **2011**, *115*, 11193−11201.

(19) Hunger, J.; Neueder, R.; Buchner, R.; Apelblat, A. A Conductance Study of Guanidinium Chloride, Thiocyanate, Sulfate, and Carbonate in Dilute Aqueous Solutions: Ion-Association and Carbonate Hydrolysis Effects. *J. Phys. Chem. B* **2013**, *117*, 615−622.

(20) Breslow, R.; Guo, T. Surface Tension Measurements Show That Chaotropic Salting-in Denaturants are Not Just Water-Structure Breakers. *Proc. Natl. Acad. Sci. U. S. A.* **1990**, *87*, 167−169.

(21) Werner, J.; Wernersson, E.; Ekholm, V.; Ottosson, N.; Öhrwall, G.; Heyda, J.; Persson, I.; Söderström, J.; Jungwirth, P.; Björneholm, O. Surface Behavior of Hydrated Guanidinium and Ammonium Ions: A Comparative Study by Photoelectron Spectroscopy and Molecular Dynamics. *J. Phys. Chem. B* **2014**, *118*, 7119−7127.

(22) Wernersson, E.; Heyda, J.; Vazdar, M.; Lund, M.; Mason, P. E.; Jungwirth, P. Orientational Dependence of the Affinity of Guanidinium Ions to the Water Surface. *J. Phys. Chem. B* **2011**, *115*, 12521−12526.

(23) Koishi, T.; Yasuoka, K.; Willow, S. Y.; Fujikawa, S.; Zeng, X. C. Molecular Insight into Different Denaturing Efficiency of Urea, Guanidinium, and Methanol: A Comparative Simulation Study. *J. Chem. Theory Comput.* **2013**, *9*, 2540−2551.

(24) Ou, S.; Cui, D.; Patel, S. Liquid-Vapor Interfacial Properties of Aqueous Solutions of Guanidinium and Methyl Guanidinium Chloride: Influence of Molecular Orientation on Interface Fluctuations. *J. Phys. Chem. B* **2013**, *117*, 11719−11731.

(25) Caleman, C.; Hub, J. S.; van Maaren, P. J.; van der Spoel, D. Atomistic Simulation of Ion Solvation in Water Explains Surface Preference of Halides. *Proc. Natl. Acad. Sci. U. S. A.* **2011**, *108*, 6838−6842.

(26) Mishra, H.; Enami, S.; Nielsen, R. J.; Stewart, L. A.; Hoffmann, M. R., III; Goddard, W. A.; Colussi, A. J. Brønsted Basicity of the Air-Water Interface. *Proc. Natl. Acad. Sci. U. S. A.* **2012**, *109*, 18679−18683.

(27) Ou, S.; Hu, Y.; Patel, S.; Wan, H. Spherical Monovalent Ions at Aqueous Liquid-Vapor Interfaces: Interfacial Stability and Induced Interface Fluctuations. *J. Phys. Chem. B* **2013**, *117*, 11732−11742.

(28) Ji, N.; Ostroverkhov, V.; Chen, C.-Y.; Shen, Y.-R. Phase-Sensitive Sum-Frequency Vibrational Spectroscopy and Its Application to Studies of Interfacial Alkyl Chains. *J. Am. Chem. Soc.* **2007**, *129*, 10056−10057.

(29) Nihonyanagi, S.; Yamaguchi, S.; Tahara, T. Direct Evidence for Orientational Flip-Flop of Water Molecules at Charged Interfaces: A Heterodyne-Detected Vibrational Sum Frequency Generation Study. *J. Chem. Phys.* **2009**, *130*, 204704.

(30) Strazdaite, S.; Versluis, J.; Bakker, H. J. Water Orientation at Hydrophobic Interfaces. *J. Chem. Phys.* **2015**, *143*, 084708.

DOI: 10.1021/acs.jpcc.7b03752
J. Phys. Chem. C 2017, 121, 23398−23405

(31) Fu, L.; Chen, S.-L.; Wang, H.-f. Validation of Spectra and Phase in Sub-1 cm^{-1} Resolution Sum-Frequency Generation Vibrational Spectroscopy through Internal Heterodyne Phase-Resolved Measurement. *J. Phys. Chem. B* **2016**, *120*, 1579−1589.
(32) Hirose, C.; Akamatsu, N.; Domen, K. Formulas for the Analysis of Surface Sum-Frequency Generation Spectrum by CH Stretching Modes of Methyl and Methylene Groups. *J. Chem. Phys.* **1992**, *96*, 997−1004.
(33) Stanners, C.; Du, Q.; Chin, R.; Cremer, P.; Somorjai, G.; Shen, Y.-R. Polar Ordering at the Liquid-Vapor Interface of n-Alcohols (C1-C8). *Chem. Phys. Lett.* **1995**, *232*, 407−413.
(34) Zhuang, X.; Miranda, P. B.; Kim, D.; Shen, Y. R. Mapping Molecular Orientation and Conformation at Interfaces by Surface Nonlinear Optics. *Phys. Rev. B: Condens. Matter Mater. Phys.* **1999**, *59*, 12632−12640.
(35) Lu, R.; Gan, W.; Wu, B.-h.; Chen, H.; Wang, H.-f. Vibrational Polarization Spectroscopy of CH Stretching Modes of the Methylene Group at the Vapor/Liquid Interfaces with Sum Frequency Generation. *J. Phys. Chem. B* **2004**, *108*, 7297−7306.
(36) Lu, R.; Gan, W.; Wu, B.-h.; Zhang, Z.; Guo, Y.; Wang, H.-f. C-H Stretching Vibrations of Methyl, Methylene and Methine Groups at the Vapor/Alcohol (n = 1 - 8) Interfaces. *J. Phys. Chem. B* **2005**, *109*, 14118−14129.
(37) Wang, H.-F.; Gan, W.; Lu, R.; Rao, Y.; Wu, B.-H. Quantitative Spectral and Orientational Analysis in Surface Sum Frequency Generation Vibrational Spectroscopy (SFG-VS). *Int. Rev. Phys. Chem.* **2005**, *24*, 191−256.
(38) Shen, Y. R. *The Principles of Nonlinear Optics*; Wiley: Hoboken, NJ, 1984.
(39) Hirose, C.; Yamamoto, H.; Akamatsu, N.; Domen, K. Orientation Analysis by Simulation of Vibrational Sum Frequency Generation Spectrum: CH Stretching Bands of the Methyl Group. *J. Phys. Chem.* **1993**, *97*, 10064−10069.
(40) Zhuang, X.; Wilk, D.; Marrucci, L.; Shen, Y. R. Orientation of Amphiphilic Molecules on Polar Substrates. *Phys. Rev. Lett.* **1995**, *75*, 2144−2147.
(41) Heinz, T. F.; Tom, H. W. K.; Shen, Y. R. Determination of Molecular Orientation of Monolayer Adsorbates by Optical Second-Harmonic Generation. *Phys. Rev. A: At., Mol., Opt. Phys.* **1983**, *28*, 1883−1885.
(42) Braun, R.; Casson, B.; Bain, C. A Sum-Frequency Study of the Two-Dimensional Phase Transition in a Monolayer of Undecanol on Water. *Chem. Phys. Lett.* **1995**, *245*, 326−334.
(43) Hore, D. K.; Beaman, D. K.; Parks, D. H.; Richmond, G. L. Whole-Molecule Approach for Determining Orientation at Isotropic Surfaces by Nonlinear Vibrational Spectroscopy. *J. Phys. Chem. B* **2005**, *109*, 16846−16851.
(44) Wu, H.; Zhang, W.-k.; Gan, W.; Cui, Z.-f.; Wang, H.-f. An Empirical Approach to the Bond Additivity Model in Quantitative Interpretation of Sum Frequency Generation Vibrational Spectra. *J. Chem. Phys.* **2006**, *125*, 133203−13.

DOI: 10.1021/acs.jpcc.7b03752
J. Phys. Chem. C 2017, 121, 23398−23405